21st Australasian Fluid Mechanics Conference
Adelaide, Australia
10-13 December 2018

Numerical investigation of wall effects on shock-induced oscillation

H. Huang[1], N. Giannelis[2], J. Geoghegan[2], G. A. Vio[2], B. Thornber[2], M. Giacobello[1], S. Lam[1]

[1]Aerospace Division
Defence Science and Technology Group, Victoria 3207, Australia

[2]School of Aerospace, Mechanical and Mechatronic Engineering
University of Sydney, New South Wales 2006, Australia

Abstract

A numerical study on the wall effects of the DST Group Transonic Wind Tunnel on self-sustained shock-induced oscillation was conducted using computational fluid dynamics. The test article was a NACA0012 aerofoil. Volume blockage effects were investigated by a parameter sweep of the chord length, and wall boundary effects were investigated by varying the porous wall inertial loss coefficient. The aerofoil mean and root-mean-square surface pressure was found to be relatively insensitive to the inertial loss coefficient, while a non-linear relationship to the chord length was observed.

Nomenclature

c	Chord length
ΔC_L	Peak-to-peak amplitude of the lift coefficient
C_P	Pressure coefficient
k	Reduced buffet frequency
H	Tunnel height (0.8m)
Δs	Nominal cell size near the aerofoil
Δt	Physical timestep
Δt^*	Non-dimensional timestep
U	Freestream velocity
y^+	Dimensionless wall distance
ω	Buffet frequency
W	Tunnel width

Introduction

Within certain flight conditions in the transonic regime, interactions between shock waves and boundary layers produce periodic flow-field oscillations. These shock-induced oscillations (SIO) generate fluctuating structural loads which may have detrimental effects to both aircraft handling quality and structural fatigue life.

SIO is a phenomenon that is well-documented and observed, however its underlying physics are not well understood, with various explanations for the phenomena provided in the literature, but none universally accepted [3]. Future experimental studies on SIO by DST Group will benefit from an *a priori* numerical assessment to aid in sensor selection and estimation of tunnel wall effects. Whilst larger test articles better facilitate instrumentation and Reynolds number matching, they also result in increasing interactions with the tunnel walls, which disturb the flow field [8].

The DST Group Transonic Wind Tunnel (TWT) is a continuous fan-driven facility capable of reaching Mach 1.3. The working section has nominal dimensions of 2.5 m length, with a nominal square cross-section of 0.8 m width. The cross-section gradually expands downstream to accommodate the growth of boundary layers. Supersonic speeds are achieved through the use of slots in the walls, allowing flow to escape to the surrounding plenum chamber, which is evacuated. Figure 1 shows an outline of the tunnel slots with flow direction being in the positive *x*-direction.

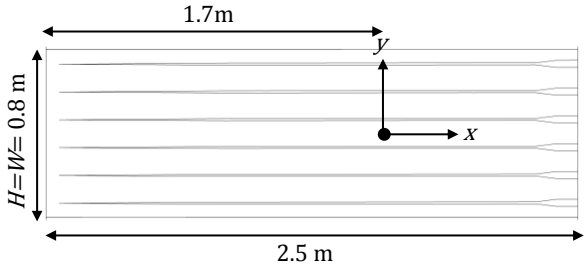

Figure 1: Outline of the TWT working section side view showing a slotted wall. The origin is placed at the centre of the TWT Schlieren window position.

A number of earlier studies have demonstrated that computational fluid dynamics (CFD) simulations, based on the unsteady Reynolds averaged Navier-Stokes (URANS) modelling approach is capable of capturing SIO, albeit with a high degree of sensitivity to the choice of turbulence model [3].

Gabaruk et. al performed a numerical investigation of flow over an RAE 2822 aerofoil with a tunnel width to chord length aspect ratio of $W/L = 3$, and noted significant solid side-wall effects [1]. Golestani et. al investigated the effects of wall porosity on the SC0410 supercritical aerofoil subject to forced pitching oscillation, and found that increasing wall porosity increased pressure fluctuation and decreased shock strength [5]. Thiery & Coustols numerically investigated a OAT15A aerofoil in both 2D and 3D within a solid-walled tunnel. The 2D simulations showed a significantly reduction in lift fluctuation compared to the freestream case, whilst the 3D case, of aspect ratio $\frac{W}{L} = 3.5$, did not [9]. Goffert et. al experimentally studied wall ventilation effects on a NACA0012 aerofoil with an aspect ratio of 3.6, exhibiting three-dimensional effects revealed by pressure sensitive paint [4].

As a low-computational cost preliminary assessment, this study investigated the wall effects of the TWT on SIO by solving the 2D URANS equations using ANSYS Fluent 18.1. Firstly, the numerical methodology was validated in a freestream grid on the NACA0012 aerofoil, for which experimental validation data is available [7]. Secondly, using a multiblock grid, the tunnel wall effects were modelled using the porous zone condition within Fluent. The effects of aerofoil size relative to the tunnel were then investigated by a parameter sweep of the aerofoil chord length. A study of various inertial loss coefficients for the porous zone was also performed.

Geometry and meshing

As a large number of grids were needed, meshing was automated using Pointwise 18.0's Glyph2 interface.

The freestream mesh was an O-grid topology, generated via hyperbolic extrusion. The tunnel mesh was a multiblock topology, with an inflation layer transitioned to a H-grid. For both topologies, the first cell height on the aerofoil was $y^+ \approx 1$. For the tunnel mesh, the first cell height at the tunnel walls was $y^+ \approx 100$, and the aerofoil was geometrically centred approximately 2/3rds downstream of the inlet, at the nominal location of the TWT Schlieren windows. Figure 2 shows the tunnel mesh near the inflation layer (left) and in the plenum (right).

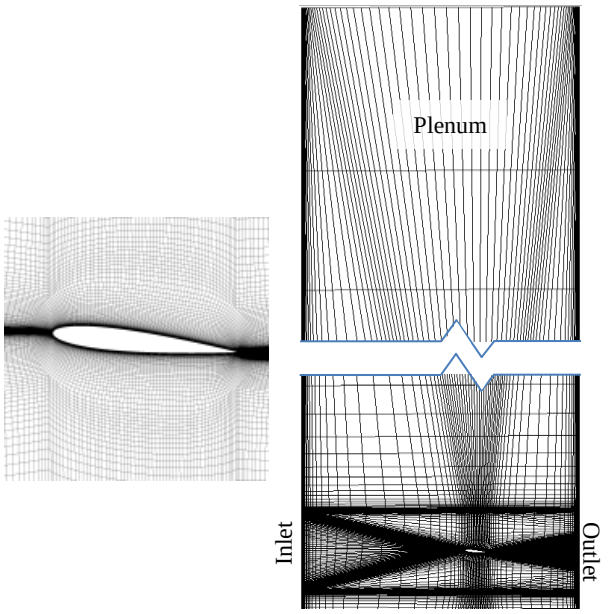

Figure 2: Multi-block mesh showing the inflation layer (left), working section and plenum (right)

Flow condition

The flow condition tested was data set 6 of McDevitt & Okuno, defined by a Reynolds number, Mach number, and angle-of-attack of $\mathrm{Re} = 10^7$, $M = 0.72$ and $\alpha = 6°$, respectively [8]. This data set was chosen because of efforts by its authors to minimise tunnel interference effects, and also due to its location deep inside the envelope of buffeting flight conditions [3].

The freestream temperature was 308K to match the tunnel conditions at the given Mach number. The boundary condition pressure was varied to keep the Reynolds and Mach numbers constant when the chord length was varied.

Solution modelling

The implicit 2D pressure-based Navier-Stokes equations were solved with second-order discretisation for all flow quantities. Taylor series-based solution extrapolation was used to accelerate convergence in the unsteady sub-iterations, and the warped face gradient correction scheme was employed. The second-order bounded scheme was used for temporal discretisation, with a non-dimensional timestep of $\Delta t^* = 0.002$ defined as:

$$\Delta t^* = \frac{\Delta t \cdot U}{c} \cdot \tag{1}$$

Turbulence was modelled using the $k-\omega$ Reynolds Stress Model. The turbulence model and time-step were taken from the validation by Giannelis [3] for the same experimental study. The simulations were run for 200 non-dimensional time units, or approximately 20 buffet cycles.

For the freestream case, the farfield extent was modelled using the pressure far-field boundary condition. For the tunnel case, the working section entrance was represented as a velocity inlet, and the exit as a pressure outlet. In the plenum, the entrance and top boundaries were defined as symmetry boundaries, whilst the exit was a pressure outlet at plenum pressure. The plenum pressure was taken from extant tunnel calibration experiments [6]

The tunnel walls were represented as a porous zone, which allows the pressure drop ΔP across the zone to be defined as a combination of inertial and viscous losses. The general expression for the model is given by:

$$\Delta P_i = -\left(\sum_{j=1}^{2} D_{ij}\mu v_j + \sum_{j=1}^{2} C_{ij}\frac{1}{2}\rho|v|v_j\right) \cdot \tag{2}$$

Where C is the inertial loss coefficient matrix, D is the viscous loss coefficient matrix, μ is the fluid viscosity, ρ is the local density and v the local velocity. As the flow is of a high Reynolds number, inertial losses dominate viscous losses, and therefore the viscous loss coefficients were neglected. The loss coefficients were also assumed to be isotropic, thus collapsing a loss coefficient matrix to a single constant. For 2D simulations, the pressure drop ΔP in each direction was therefore:

$$\Delta P = C_2 \times \left(\frac{1}{2}\rho|v|\sum_{j=1}^{2} v_j\right) \cdot \tag{3}$$

As there were no experimental data available with which to calculate C_2, three different values of C_2 were tested spanning two orders of magnitude. The porous zone porosity was taken to be 0.0726, an approximation of the true porosity of the tunnel walls. The porosity was also assumed to be isotropic. As the physical porosity of the tunnel walls is anisotropic, the porous zone model can therefore only capture bulk flow effects.

Freestream aerofoil reference case

Before investigating porous wall effects, the numerical solution model was firstly verified with the aerofoil in the freestream. As no experimental chord-wise pressure distribution is available, validation was by comparison to the reduced buffet frequency *k*, defined as:

$$k = \frac{\omega c}{U} \cdot \tag{4}$$

Table 1 shows the freestream grid test matrix and results. Grid convergence was assessed using the reduced buffet frequency k, peak-to-peak amplitude of the lift coefficient ΔC_L and the time-averaged pressure distribution on the chord, shown in Figure 3. Convergence was obtained at a mesh resolution of $\Delta s/L = 0.01$. The buffet frequency was slightly over-predicted, but exhibited agreement with the experimental value. An instantaneous Mach number flow field in the buffet cycle at this resolution is presented in Figure 4.

Nodes (K)	$\Delta s/c$	k	ΔC_L (dB)
80	0.02	0.58	-29.34
100	0.01	0.58	-25.13
150	0.005	0.58	-25.06
McDevitt & Okuno [7]	N/A	0.55	N/A

Table 1: Freestream test matrix

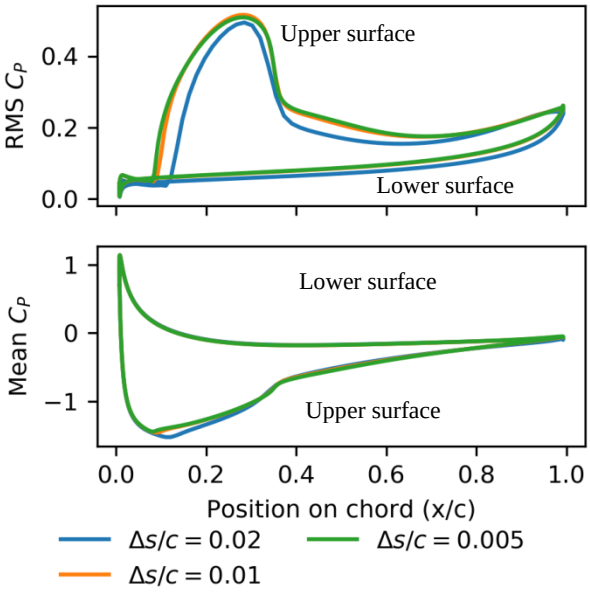

Figure 3: Pressure distribution along the aerofoil

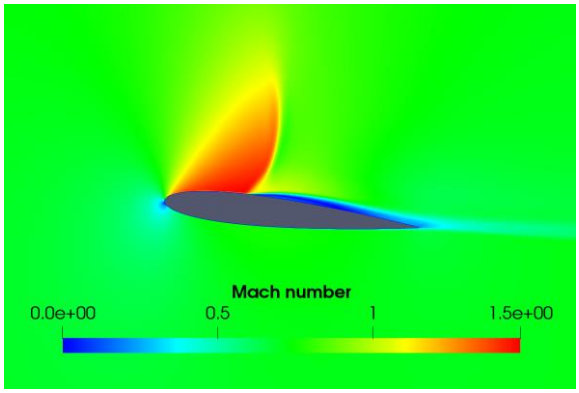

Figure 4: Instantaneous Mach number flow field for the freestream case at $\alpha = 6°$

Porous wall

Table 2 shows the test matrix for the porous wall case, with the test cases for a grid convergence study (upper), sweep of chord length (middle), and variation of inertial loss coefficient (lower). Here the chord length variation is expressed as a tunnel height-to-chord, H/c, aspect ratio. Figure 5 shows the pressure distribution over the aerofoil for the grid convergence study. Similarly to the freestream case, grid independence was reached at a mesh resolution of $\Delta s/c = 0.01$, and was used for subsequent simulations. Figure 6 shows the instantaneous Mach number flow field for that resolution and $H/c = 3.5$.

C_2	$\Delta s/c$	Nodes (K)	H/c
0.1	0.02	189	3.5
0.1	0.01	223	3.5
0.1	0.005	308	3.5
0.1	0.01	247	5.5
0.1	0.01	251	6.5
0.1	0.01	261	7.5
1.0	0.01	223	3.5
10.0	0.01	223	3.5

Table 2: Test matrix for the porous wall case showing convergence study (top), chord length parameter sweep (middle) and porous wall loss coefficient variation (bottom)

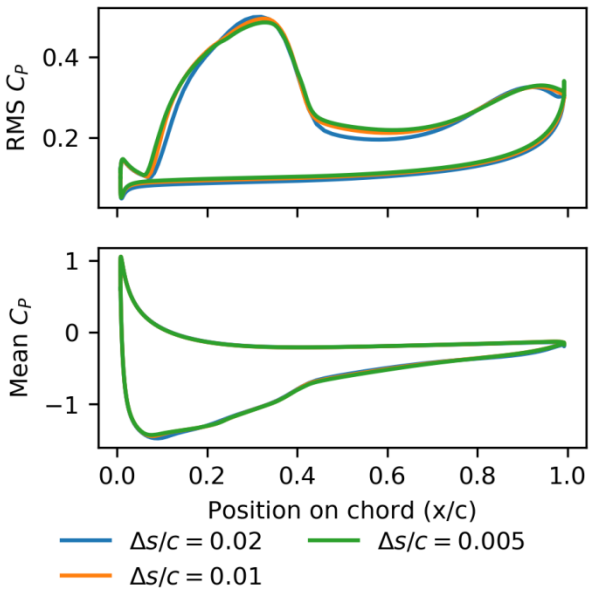

Figure 5: Pressure distribution along the aerofoil for the porous wall grid convergence study

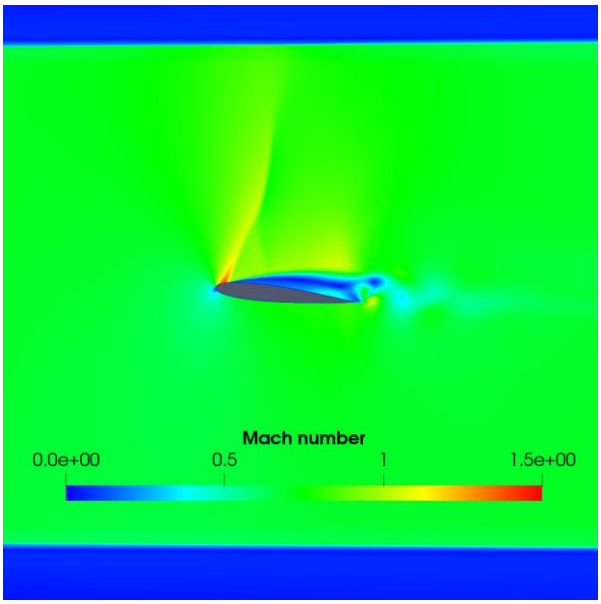

Figure 6: Instantaneous Mach number flow field for the porous wall case for $H/c = 3.5$, and $\alpha = 6°$

Figure 7 shows the sensitivity of the chord-wise pressure distribution to volume blockage by varying the chord length, expressed as H/c. As the chord length is decreased, the RMS pressure reduces, and the mean shock position moves upstream. However, the pressure profile does not approach the freestream case monotonically. This is likely due to the non-linear effects as a combination of shock-wall interaction, and volume blockage. Further reduction in chord size may be required before the tunnel wall effects become insignificant. Furthermore, the TWT Mach number is controlled via a combination of the main tunnel fan and plenum evacuation. Therefore, future studies may explore the wall effects for other tunnel conditions at the same Mach number.

Figure 8 shows a pseudo-schlieren ($\partial\rho/\partial x$) comparison between the freestream case and $H/c = 7.5$, the smallest chord size investigated, where the reflection of weak acoustic waves at the porous wall are seen.

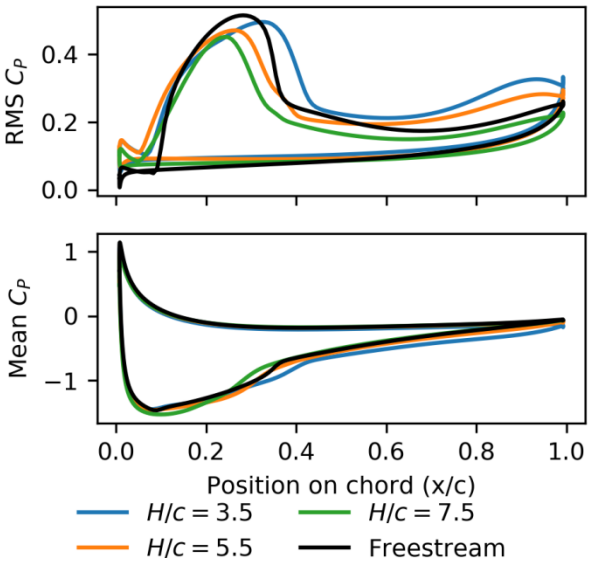

Figure 7: Pressure distribution over the aerofoil for the sweep of *c*

Changing the inertial loss coefficient had negligible effect on the pressure distribution (and is not shown). A possible reason is the low pressure drop of 109 Pa from the tunnel working section to the plenum chamber and requires further investigation. Increasing the plenum evacuation at the same Mach number to achieve a higher pressure differential between the working section and plenum may result in a greater sensitivity of the flow to the inertial loss coefficient.

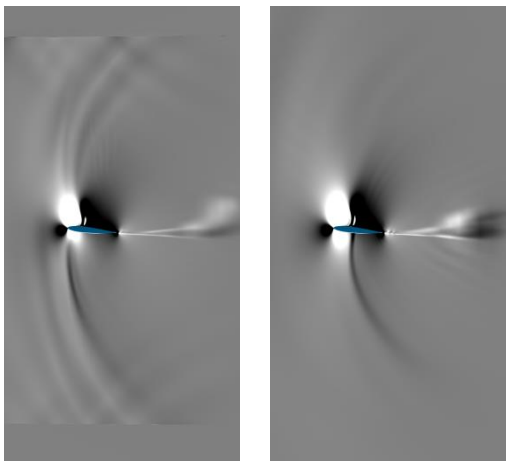

Figure 8: Schlieren visualisation of freestream (left) and porous wall (right) simulations, with the aerofoil coloured in red.

Conclusion

A preliminary numerical investigation of slotted tunnel wall effects on shock-induced oscillation using the porous media model within ANSYS Fluent was performed. The effects of volume blockage were found to be non-linear. With a low pressure drop across the wall, the flow was found to be insensitive to the inertial loss coefficient parameter. The porous wall model produced weak acoustic reflections.

Investigation of a larger test matrix, including smaller chord sizes and different plenum pressures, as well as holding the physical flow condition constant whilst varying the tunnel dimensions, are future avenues of exploration which may yield further insights.

Acknowledgements

The authors acknowledge Benjamin Loxton from Advanced VTOL Technologies for his valuable insight.

References

[1] Gabaruk. A., Shur. M, Strelets. M. & Spalart, P., *Numerical Study of Wind-Tunnel Wall Effects on Transonic Airfoil Flow*, *AIAA Journal*, 41, 6, 2003.

[2] Giannelis, N. & Vio, G, *Transonic shock buffet of aerofoils*, The University of Sydney, 2017.

[3] Giannelis, N., Vio, G. & Levinski, O, A review of recent developments in the understanding of transonic shock buffet, *Progress in Aerospace Sciences*, 92, 39-84, 2017.

[4] Goffert, B., Ortega. M. & Falcao Filho, J., Wall Ventilation Effects upon the Flow about an Airfoil in a Transonic Wind Tunnel, *Experimental Techniques*, 40, 2, 461-481, 2003.

[5] Golestani, A., Soltani, M & Masdari, M., Effect of wind tunnel wall porosity on the flow around an oscillating airfoil at transonic speeds, *Scientia Iranica B*, 24, 3, 1069-1076, 2017.

[6] Lam, S., Loxton, B., & Dawes-Lynch, J., *Characterisation of the DST Group Transonic Wind Tunnel via a centreline pipe* (in preparation), 2018.

[7] McDevitt, B. & Okuno, A., *Static and Dynamic Pressure Measurements of a NACA 0012 Airfoil in the Ames High Reynolds Number Facility*, NASA, 1985.

[8] Rasuo, B., On status of wind tunnel wall correction, *25th Congress of the International Council of the Aeronautical Sciences*, 2006.

[9] Theiry, M., Coustols, E., Numerical prediction of shock-induced oscillations over a 2D airfoil: Influence of turbulence modelling and test section walls, *International Journal and Heat and Fluid Flow*, 27, 661-670, 2006.